PERFORMANCE ANALYSIS OF A HYBRID-ELECTRIC RETROFIT OF A RUAG DORNIER DO-228NG

P. G. Juretzko[1], M. Immer[1] and J. Wildi[2]

[1]ALR Arbeitsgruppe für Luft- und Raumfahrt, Gotthardstr. 52, 8002 Zurich, Switzerland
[2]RUAG Aviation, Seetalstrasse 175, 6032 Emmen, Switzerland

Abstract

In projects such as the Airbus E-Fan, the Siemens Magnus eFusion or the Pipistrel Taurus G4 [1], electric propulsion systems have successfully been installed in small aircraft in the 2-4 passengers class. Electric propulsion opens up new operational concepts due to their potential to reduce noise emissions. By significantly reducing take-off and approach noise, electric airplanes can operate at airports less dependent on local airport operation restrictions. The considerable range disadvantage of purely electric aircraft can be overcome by hybrid-electric propulsion solutions [2], making "new concepts" feasible in the near term. These concepts are particularly interesting when looking at larger aircraft that are intended to carry more passengers or payload, e.g. the 20 passengers class.

The goal of this work is to conduct the sizing of a hybrid-electric propulsion concept based on the retrofit of a RUAG Do-228NG and to investigate the resulting performance. A methodology that is capable of obtaining the desired results has been presented in [3]. In cooperation with RUAG Aviation, a flight performance model of the Do-228NG is developed and validated as a baseline. This model is modified to account for changes related to the retrofit of a hybrid-electric propulsion system. Finally, mission performance of the retrofit model is simulated and compared to the baseline aircraft.

1. INTRODUCTION

Future aircraft programs face ambitious emission goals compared to the levels that occur today. The EU Commission has, for example, published a reduction target of -65% for perceived noise levels in its Flightpath 2050 document [4].

A main source of aircraft noise emissions is the propulsion system. Since electric propulsion systems cause significantly less noise emissions, these may help to achieve the mentioned goals.

The application of electric propulsion systems to small aircraft in the 1-4 passengers class has been successful in the recent past [1, 5, 6, 7]. One of the upcoming steps in using electric propulsion systems is their application to larger aircraft, such as the 20 passengers class. In comparison to fuel-based propulsion systems, however, pure-electric propulsion concepts have significant range disadvantages as long as the reachable energy density in current batteries does not improve significantly [2].

A possible compromise to the aforementioned problem may be the application of hybrid-electric propulsion systems that benefit from the advantages of both propulsion technologies. Fuel-based propulsion offers good cruise range performance while electric propulsion technologies may reduce noise emissions significantly. Before significant investments in a full-scale development program are necessary, the benefits and implications of such a propulsion concept could be investigated by realizing a retrofit of existing hardware in the mentioned class.

Since the hybrid-electric system design will have significant influence on the mission performance of the retrofitted aircraft, these will have to be studied carefully. During these studies, simple operating modes such as pure-conventional, pure-electric or parallel modes may be analyzed with established methods of various levels of detail. However, studies of hybrid-electric propulsion modes that include charging, discharging or sustained operation require more advanced methodologies since design missions or scenarios become non-trivial through additional degrees of freedom. [3]

This work presents a methodology that allows to perform the mentioned analyses. This methodology is applied to investigate the retrofit of a hybrid-electric propulsion system to the RUAG Do-228NG [8]. Initially, the sizing of the hybrid-electric system is analyzed. Then, feasible scenarios for this specific retrofit, such as hybrid-electric ("silent") take-off, "silent" landing as well as "silent" surveillance or patrol tasks are evaluated.

After the explanation of the methodology and simulation details in Section 2, the investigated aircraft as well as calculated mission scenarios are described in Section 3. This is followed by a presentation and discussion of the results in Section 4. The work is completed with a conclusion covering the methodology and findings in Section 5.

2. METHODOLOGY

This section provides an overview of the methodology, and the assumptions that will be used to compute electric and hybrid-electric aircraft performance.

2.1. Performance Equations

The derived performance equations are based on Newton's second law, which states that the rate of change of momentum is proportional to the applied forces

(1) $\quad \dfrac{dp}{dt} = \sum F_{ext}$,

where p is the momentum, defined as the mass m multiplied by the velocity v, and F_{ext} the external forces. By neglecting the rotational dynamics (point mass assumption), the quasi-stationary performance equations can be derived. Furthermore, we use the assumption that the rate of change of the external forces is small, (e.g.: $\frac{d(mg)}{dt} \ll 1$) and the motion is restricted to the vertical (or horizontal) plane. The equations of motion in the airplane fixed coordinate system (Fig. 1) can be formulated in the flight-path angle γ and radial (lift) direction as

(2) $\quad m\dot{v} + D - T\cos(\alpha + \sigma) + mg\sin(\gamma) = 0$

and

(3) $\quad -mv\dot{\gamma} + L + T\sin(\alpha + \sigma) - mg\cos(\gamma) = 0$

respectively, where T is the thrust force, D the drag force, L the lift force, α the angle-of-attack and σ the thrust incidence angle.
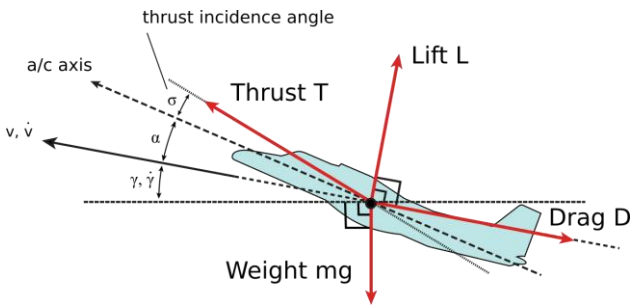

FIGURE 1. Forces acting on the point mass in the vertical plane

Generally, the mass *m* of the airplane only changes by the fuel flow

(4) $\quad \dfrac{dm}{dt} = -\dot{m}_f$.

The electric energy stored in the battery, *E*, changes by the net power consumption

(5) $\quad \dfrac{dE}{dt} = -P_{net}$,

where P_{net} can be positive (discharging) and negative (charging).

Together with the kinematic equations

(6) $\quad \dot{x} = v\cos(\gamma)$

and

(7) $\quad \dot{z} = -v\sin(\gamma)$,

that relate the speed and the flight path angle to the horizontal and vertical velocity, the resulting set of (first- and second order) ordinary differential equations (ODEs) can be readily solved by any modern numerical mathematics package.

Note that the performance equations are independent of the modelling approach for the parameters T, D, L, $\dot{m}_f$ and P_{net}.

2.2. Performance Model

The performance model consists of an aerodynamics model and a propulsion model. For this example, we only consider the serial-hybrid electric propulsion model. For other architectures, the equations are slightly different, however the main modelling approach remains the same. In addition, the operating weight empty (OWE) of the aircraft (including the battery), the payload mass and the fuel mass complete the model.

2.2.1. Aerodynamics

Lift and drag forces (L and D in Eq. 2 and 3) are commonly modelled in non-dimensional form:

(8) $\quad L = C_L \dfrac{1}{2}\rho v^2 S_{ref}$

(9) $\quad D = C_D \dfrac{1}{2}\rho v^2 S_{ref}$

with $\frac{1}{2}\rho v^2$ being the dynamic pressure, S_{ref} the aerodynamic reference area, C_L and C_D the lift- and drag coefficients respectively. The lift coefficient can be written as a function of angle-of-attack α and the Mach number

(10) $\quad C_L = f(\alpha, M)$

and the drag coefficient can be split into a lift-independent and lift dependent part

(11) $\quad C_D = C_{D0}(M,h) + C_{Di}(C_L, M)$

as functions of the Mach number M the altitude h and lift-coefficient C_L.

2.2.2. Propulsion

The propulsion architecture for a serial-hybrid electric propulsion system is depicted in Figure 2.
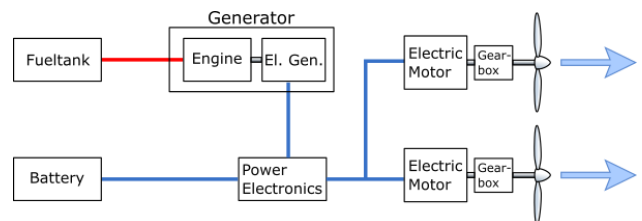

FIGURE 2. Serial-hybrid propulsion architecture with two propellers driven by electric motors.

For propeller propulsion, thrust can be obtained with the non-dimensional propeller thrust coefficient C_T as

$$(12)\quad T = C_T \rho n^2 D_p{}^4 \,,$$

where n is the propeller speed (revolutions per time) and D_p the propeller diameter. The power required by the propeller can be obtained with the non-dimensional propeller power-coefficient C_P as

$$(13)\quad P_{req} = C_P \rho n^3 D_p{}^5 \,.$$

The propeller can therefore be fully characterized by the two parameters

$$(14)\quad C_P = f(J,\beta,M)$$

and

$$(15)\quad C_T = f(J,\beta,M) \,,$$

where J is the advance ratio, β the propeller blade angle and M the Mach number.

The electric power consumption of the electric motor is therefore defined using the propeller power required (Eq. 13) as

$$(16)\quad P_{Mot} = P_{req}/\eta_{Mot} \,.$$

The efficiency of the electric motor may be defined by using either a constant or a map. The motor efficiency map is dependent on the motor speed n and the torque Q:

$$(17)\quad \eta_{mot} = f(n,Q) \,.$$

The generator unit consists of an engine and an electric generator. The fuel flow of the generator unit is provided as a function of the installed shaft power P_{Engine},

$$\dot{m}_{f,Gen} = f(P_{Engine},h,v,n) \,,$$

where h is the altitude, v the velocity and n the engine speed. The electric power output is therefore defined as

$$(18)\quad P_{Gen} = P_{Engine} \cdot \eta_{Gen} \,,$$

where η_{Gen} is, analogous to the electric motor efficiency (Eq. 17), either a constant or a map.

Finally, the net battery power consumption may be written as

$$(19)\quad P_{net} = \frac{N \cdot P_{Mot} - P_{Gen} + \sum P_{Consumers}}{\eta_{bat}} \,,$$

where N is the number of electric motors / propellers and $P_{Consumers}$ additional electric consumers such as avionics.

The battery charge or discharge efficiency η_{bat} is modelled as

$$(20)\quad \eta_{bat} = f(P_{net}) = \begin{cases} \eta_{bat,discharge} & if \quad P_{net} > 0 \\ 1/\eta_{bat,charge} & if \quad P_{net} < 0 \end{cases} \,.$$

2.3. Simulation Environment

To simulate point and mission performance, the Aircraft Performance Program APP is used [9]. APP implements the performance equations described in Section 2.1 and provides input capabilities for the parameters described in Section 2.2 [10]. For a given flight state, APP numerically solves the 2D point mass equations (Eq. 2 and 3). Furthermore, for a constant speed propeller, the propeller blade angle (Eq. 14 and 15) is solved together with the motor power setting to obtain the required thrust. This is achieved by setting the motor shaft power equal to the propeller power required and iterating over the blade angle.

For mission performance simulation, APP uses a Runge-Kutta forth-order numerical integration to compute the position, altitude, velocity, fuel mass and battery energy.

APP implements a standard atmosphere model[1] according to [11] that can be customized.

The APP version 7 implements parallel and serial hybrid electric propulsion models. Figure 3 shows the different operating modes APP provides for the generator.
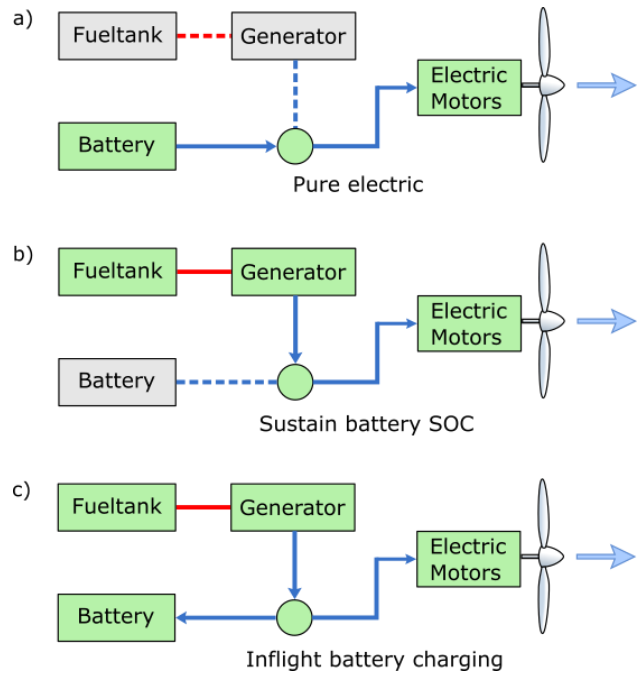

FIGURE 3. Operating modes of the serial electric propulsion system. Pure electric propulsion (a), sustained battery state-of-charge (b) and recharging while inflight (c).

For purely electric flight, the generator is switched off (Fig 3a). In order to sustain the battery energy (Fig 3b), the

---

[1] https://github.com/ALR-Aerospace/pyAPP6Tools

output of the generator is matched to the total electric power consumption

$$(21) \quad P_{net} = N \cdot P_{Mot} - P_{Gen} + \sum P_{Consumers} = 0 \,,$$

and solved for the power setting of the generator's engine. If the power setting is lower, the battery is drained, and if it is higher, the battery is charged (Fig. 3c).

For complex sizing and performance studies, APP's command line interface is used together with the Python [12] module *pyAPP*[2]. This setup has the advantage of using APP's validated computation core, including the generator power solver and mission range solver, by coupling it with the flexible scripting language Python [3].

3. CASE SETUP

This section gives an overview of the investigated aircraft and describes the calculated mission profiles.

3.1. Aircraft

The baseline aircraft for the calculations in this work is the RUAG Do-228NG, a versatile turboprop platform for passenger and cargo transport as well as special mission applications. The aircraft features a high-wing design with a conventional tail configuration and unpressurized cabin. The general arrangement and principal dimensions are depicted in Figure 4. The most important weight characteristics are listed in Table 1.
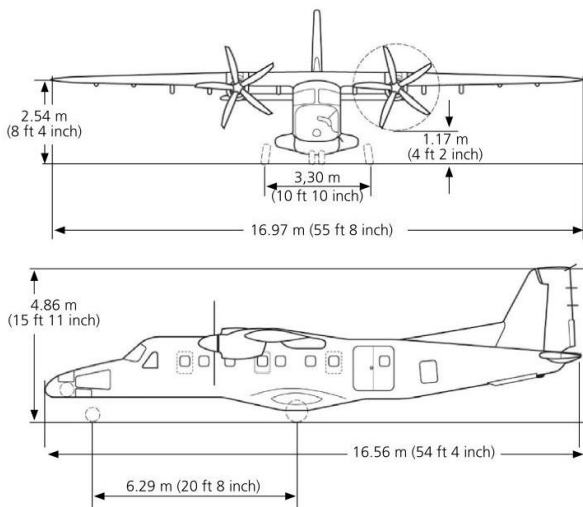

FIGURE 4. The general arrangement and dimensions of the RUAG Do-228NG. [8]

Weights	[kg]	[lbm]
Aircraft Weight Empty, no engines	3'550	8'598
Turboprop Engines	350	771
Maximum Fuel Weight	1'885	4'156
Maximum Payload	2'040	4'498
Max. Take-off Weight (=MTOW)	6'400	14'110

TAB 1. Weight characteristics of the Do-228NG. [8]

For the presented studies, mostly manufacturer data was

[2] http://aircraftperformance.software/pyapp/

used to create a performance model. The completed model includes aerodynamic data, mass and propulsion system performance.

Besides the available data of the baseline aircraft, the analysis of the retrofit required a full modeling of the hybrid-electric propulsion system. This includes the battery system, the electric motors, the fuel-based generator and the propeller.

The battery model is defined by a specific energy density E_s, usually provided as available energy capacity per battery weight. State-changes, such as charging or discharging, are calculated according to the Equations (5) and (19). The energy density of the battery system for this retrofit analysis was estimated at $E_s = 150$ Wh/kg. This value is comparable to the realized energy densities found in small electric aircraft [13]. At the same time, it leaves a margin to the energy density that was achieved in high-performance applications, such as the battery-system that was realized in the Solar Impulse 2 aircraft [14]. Charge and discharge efficiencies are assumed as 98%.

The electric motor modelling is mainly depending on the available power-density of the motor. Recent motor designs and applications have proven that a power-density of 5.2 kW/kg is feasible with the current technology level [7, 15]. The manufacturer states that this design is scalable up to the power-class of about 1 MW of installed shaft power. Therefore, the electric motor is modelled with an installed power-density of 5 kW/kg. The electric motor mass is scaled from derived properties of the aforementioned design to match the SLS installed shaft-power of about 1160 kW (1554 SHP) of the two down-rated Garrett TPE331 turboprop engines that are installed in the baseline Do-228NG [8]. This leads to an installed motor weight of 116 kg, each. The operating efficiency of the electric motors is set to 95%. This efficiency level has been demonstrated on a test-bench setup [15]. The efficiency of the power-electronics is also estimated at 95%.

The generator model defines the relationship of resulting generator power and related fuel flow. In this model, a Wankel-type rotary internal combustion engine is assumed. The specific fuel consumption is assumed at constant 300 g/kWh. The mass of the generator model is estimated with a power-density 3.5kW/kg. The combustion-engine power-loss with altitude is modelled as defined in Equation (22) [16]. Power off-takes and further losses are assumed to account for 5% of available shaft power.

$$(22) \quad P(h) = P_{SL} \left(\frac{\rho}{\rho_0} - \frac{1 - \rho / \rho_0}{7.55} \right)$$

The propeller was modeled with available manufacturer data for the thrust- and power-coefficients as defined in the Equations (14) and (15).

The weight build-up of the retrofit model, as depicted in Table 2, shows that battery, generator and available fuel-load are defined by the design decision for battery weight and generator size.

Weights	[kg]	[lbm]
Empty	3'550	7'820
Electric Motors	232	511
Payload (50 %)	1'020	2'247
Battery & Generator	from sizing	
Fuel load	difference to MTO	
Take-off Weight (=m_{TO})	6'400	14'110

TAB 2. Weight build-up of the retrofitted Do-228NG.

When defining a design point, battery mass and installed generator power are chosen. The maximum fuel mass m_{fuel} is then limited by payload, installed battery mass and generator mass. This relation is defined by the following equation:

$$(23) \quad m_{fuel} = m_{TO} - m_{Bat\&Gen} - m_{Payload} - m_{motors} - m_{empty}$$

This means that a specific weight build-up is defined for each hybrid-electric design point that is simulated with the presented methodology.

3.2. Mission Profile Descriptions

An overview of the simulated mission profiles is given in Figure 5. The illustrations specified as a) and b) comprise climb calculations only, these end at a defined top-of-climb (TOC).

Figure 5a illustrates a climb profile with either all-electric or all-hybrid propulsion. All-electric means only battery energy is used to deliver propulsive energy to the electric-motors, see Figure 3a. All-hybrid propulsion means the battery and the generator deliver power to the electric motors at all times. This all-hybrid mode is depicted in Figure 3c, where the energy flux originates from the generator, leading towards the electric motors (opposite to the indicated arrow). The result of interest is reachable climb altitude.

Figure 5b illustrates a climb schedule that includes a change in operating mode during the climb. The calculation is performed with pure-electric mode (Fig. 3a) up to the "activation altitude", where the generator is activated to reach a higher altitude before the battery is completely discharged (Fig. 3c). The result of interest is reachable climb altitude.

Sketches 5c, d and e indicate the profiles of a full mission simulation, including the most important requirements for operating modes and battery state-of-charge (SOC). These sketches resemble possible applications of a Do-228NG retrofit, for example a transport profile with "silent" (i.e. electric) take-off and landing or surveillance scenarios, such as pollution control, border patrolling or wildlife surveillance. These profiles are calculated with a defined generator power and battery mass so that the resulting performance of such a retrofit for feasible but simple scenarios is obtained.

The profiles shown in Figure 5c and d are almost identical. The climb is calculated as indicated in Figure 5b, so that the generator activation altitude (4'000 ft) is reached by using only battery energy. Then, the generator is switched on and the climb is continued up to the top-of-climb altitude (6'000 ft). Battery SOC is 10% at the end of the climb (TOC). After an acceleration to cruise speed (160 KCAS), the battery is charged during the following cruise segment. Then, a cruise segment with sustained SOC (Fig. 3b) follows. The cruise segment is followed by a sustained descent to 4'000 ft. At an altitude of 4'000 ft, the generator is switched off and a pure-electric descent follows. Note that the charging segment is defined so that the battery SOC reaches 10% or 90% at the end of the mission. The result of interest is maximum range with a noise-reduced take-off, climb, descent and landing. For the mission profile in Figure 5d, an SOC of 90% at landing was chosen because it may be operationally relevant to be able to start a return-leg soon after arrival.

The mission profile depicted in Figure 5e shows a different mission type. The climb and the descent profiles are simulated by only using generator power (sustained mode, Fig. 3b). The climb is followed by a sustained ferry flight towards a given area of interest. Then, the generator is switched off and a loiter segment in pure-electric mode (Fig. 3a). The loiter segment stops when the battery SOC reaches 10%. The return-flight and descent are simulated in sustained mode. Result of interest is the maximum electric loiter time and the radius of action.

The reserves for the profiles c, d and e are 30 minutes of loiter at minimum fuel flow and 5% of initial fuel load at the end of the mission.
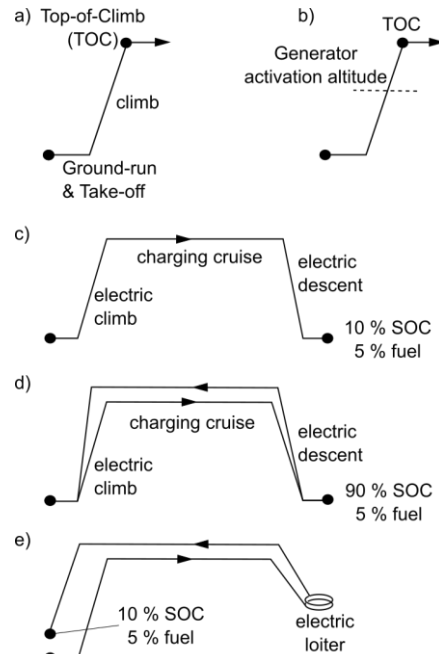

FIGURE 5. An overview of the simulated climb and mission profiles. Reserves for profiles c, d and e are 30 minutes of loiter and 5 % of initial fuel.

4. RESULTS AND DISCUSSION

This section describes the obtained results for the profiles as specified in Section 3.2. At first, three examples show climb performance studies of possible retrofits and different operating modes. These studies lead to the selection of a possible design point. This design point is

then used to analyze the resulting mission performance of the three different mission profiles depicted in Figure 5c, d and e.

Note that all results that are presented in this section are calculated with a fixed take-off weight of 6400 kg. The specific energy density of the battery is set to 150 Wh/kg for all examples. Battery mass, generator mass and fuel mass are defined as specified in Section 3.1 and Equation (23).

4.1. Top of Climb Altitude Using Battery Energy

In a first example, the presented method and the developed model is used to calculate pure-electric climb performance with a profile similar to Figure 5a. The result of interest is the altitude that may be reached by using only the electric energy that is stored within the batteries. This means the generator does not provide any power to the propulsion system or the battery (Figure 3a).

The calculated climb profile consists of a take-off ground run with subsequent acceleration to 125 KCAS and climb at constant CAS until battery state of charge (SOC) reaches 10%. The results are presented in Figure 6.
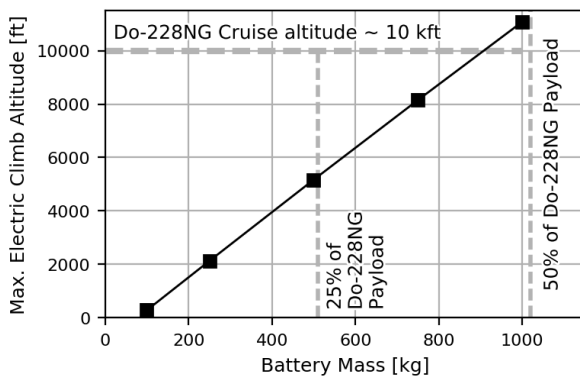
FIGURE 6. Maximum reachable climb altitude by using only battery energy while discharging the battery to 10% SOC. Take-off weight is 6'400kg.

The maximum reachable altitude correlates linearly with available energy, i.e. installed battery mass.

The usual cruise altitude of the baseline aircraft Do-228NG is about 10 kft. Results indicate that this altitude could be reached with a battery of about 900 kg. Note that the maximum payload of the aircraft is 2040 kg [8]. The operational value of the results is questionable because no assessment of available payload, fuel-mass or energy reserves is made. To obtain a better understanding of these implications, the influences and advantages of other operating modes are investigated in the following sections.

4.2. Top of Climb Altitude Using Battery and Generator

The results of this example, as shown in Figure 7, are calculated for the climb profile segments as shown in Figure 5a. The only difference to the previous example is

the operating mode of the propulsion system. The battery and the generator are used to deliver propulsive shaft power from the beginning of the simulation and at the same time. A variant of this mode is depicted in Figure 3c. For this example, the energy flux needs to originate from both, battery and generator towards the electric motors. The climb segment stops when the SOC reaches 10%. This operating mode may be considered similar to a "parallel" system setup.
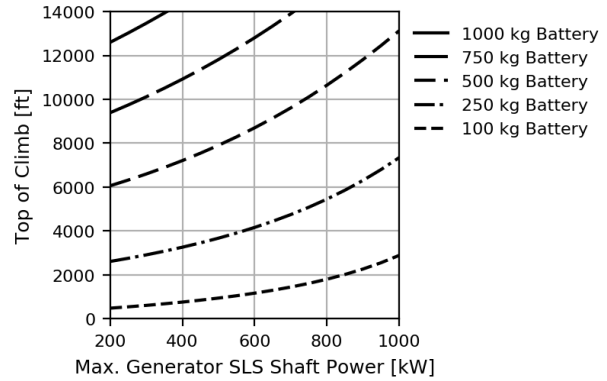
FIGURE 7. Reachable climb altitude using hybrid-electric propulsion, i.e. generator power and battery energy in parallel.

In the results as shown in Figure 7, the generator power-output and battery size are treated as variables. Obiously, the reachable climb altitude is directly proportional to these two variables. The larger the battery size, and the larger the generator power-output, the higher the reachable altitude. Note that the results for 0 kW of max. power-output of the generator are not shown here. This would, however, be identical to those of the pure-electric climb example (Fig. 6).

With increasing size of the generator, less power is provided by the battery and the reachable cruise altitude increases. The trend of the lines for constant battery weight is almost horizontal on the left hand side and assymptotically approaching a vertical line towards the region of 1.1 MW of installed generator power. This behaviour is easy to explain if we consider that a generator with 1.1 MW shaft-power provides enough propulsive power to cover the power demand of the whole aircraft during climb. This removes the need to drain energy from the battery.

Comparison of the presented results in Figure 7 with those in Figure 6 allows to say that constant hybrid-electric propulsion allows higher reachable climb-altitudes – depending on available generator power. Moreover, constant hybrid-electric propulsion allows a limited reduction of noise emissions during flight.

4.3. Activation Altitude of the Generator

This third example presents a combination of the previous two examples. The calculated climb-profile is depicted in Figure 5b. It consists of a take-off ground-run, which is followed by an acceleration to best climb-speed and a subsequent climb. Initially, only battery energy is used for propulsion (Figure 3a). The generator is activated later during the climb segment, so that a battery state of charge

of 10% is reached just at the defined top-of-climb altitude (Figure 3c, discharge mode). Consequently, the presented results are only valid for a single top-of-climb altitude.

Figure 8 illustrates the change of SOC with change of operating mode and altitude for this calculation set-up. The altitude at which the generator is activated is specified as point A. The altitude of this point is referred to as "activation altitude" in Fig. 5b. Point B indicates the altitude that would be reachable with pure-electric mode (results of Fig. 6). The line connecting the points A and C indicates the path that leads to the target SOC (here: 10%) at the desired top-of-climb altitude. This line is defined by battery mass and generator power. As indicated by the line connecting the points A and D, the slope of SOC with altitude is depending on available generator power.
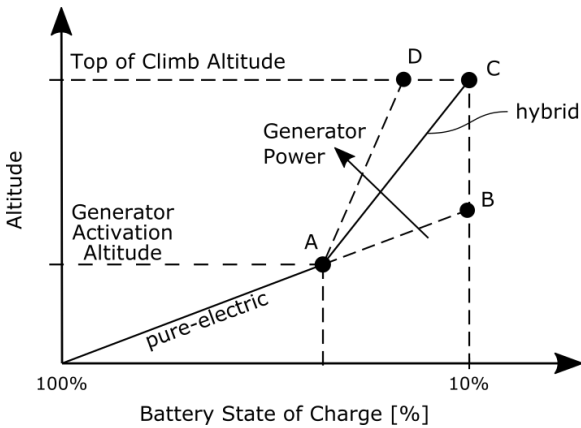

FIGURE 8. Schematic drawing illustrating the change of battery state-of-charge during a climb with changing operating mode of the propulsion system.

Due to the nature of the mentioned relationships, the presented methodology needs to be used to find the exact generator activation altitude to obtain a defined (i.e. required) activation altitude *together* with a defined top-of-climb once a hybrid-electric design point is defined. To solve this task, the simulation procedure as outlined in Figure 9 was employed. After specification of the hybrid-electric system design point, that means battery mass and generator power, the resulting weight build-up is obtained from the sizing-relations that were explained in Section 3.1. The climb profile is then calculated with an initial guess for the activation altitude. The activation altitude is then numerically adjusted until the target SOC is reached at the defined top of climb.
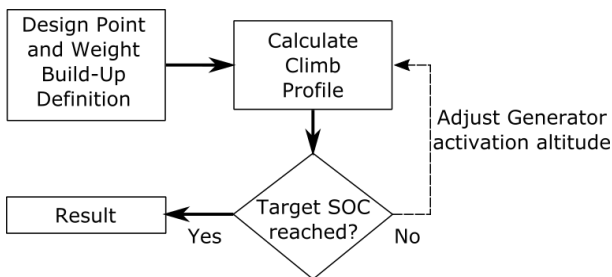

FIGURE 9. Simulation procedure to obtain the generator activation altitude resulting after defining battery mass and generator power.

A top of climb altitude of 6'000 ft was deemed reasonable for this example. The results of this calculation are depicted in Figure 10. As in the previous example, the installed battery mass and the installed generator shaft-power are varied. Lines of constant battery mass are plotted as a function of generator activation altitude and generator shaft-power. Note that take-off weight is kept constant at 6400 kg. Available payload and fuel mass are therefore reduced by installed battery mass and generator mass (see Eqn. 23).
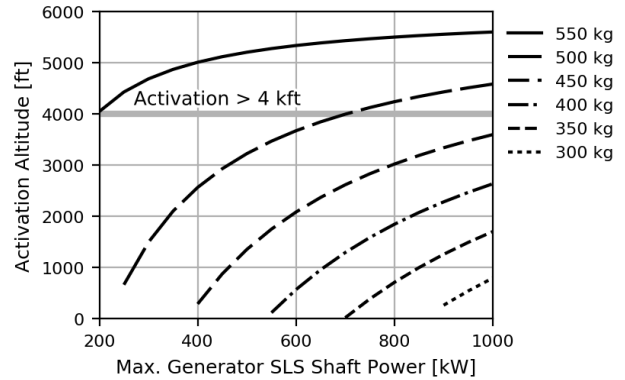

FIGURE 10. Activation altitude of the generator plotted versus installed generator shaft-power.

It is clearly visible that larger battery sizes allow for a higher activation altitude of the generator. The curvature of the lines indicating constant battery mass depends on available generator shaft power. The more shaft-power available, the less battery-energy is consumed after the generator is activated. This means that more powerful generators allow to discharge batteries further before the generator is activated. Consequently, this allows for a higher activation altitude when installed battery mass is kept constant and available generator power increases. Lines of constant battery mass approach a horizontal gradient towards about 1.1 MW of shaft power. From this point on, the generator is powerful enough to provide the shaft-power that is required to climb so that there is no battery energy required for generators of 1.1 MW shaft-power or higher. An increase in battery weight has no more effect on activation altitude if a powerful generator is used. Note that the results for an installed generator shaft power of 1.1 MW are identical to those shown in Figure 6.

If an exemplary generator activation altitude of 4'000 ft is assumed as requirement, the valid solutions for minimum required battery mass and minimum required generator shaft power can be read directly from the chart (see 4 kft indication in Figure 10). Comparing the results to those of Figure 6 show that the required battery mass to reach an altitude of 6'000 ft can be reduced from about 580 kg to about 500 kg (minus 14%) if a generator with 700 kW at SLS would be chosen and activated above 4'000 ft.

Note that the presented chart is only valid for the defined top-of-climb altitude of 6'000 ft.

4.4. Generator and Battery Sizing Constraints

To this point, only the influence of battery size and generator power on climb performance was studied. Before looking at mission performance, it is essential to

understand further constraints to the selection of these design variables.

For the following studies, the minimum payload requirement is assumed 1020 kg, this is 50% of the payload capability of the baseline Do-228NG. This means that the battery and the generator (along with related sub-systems) are limited to 1020 kg.

Depending on the desired operational flexibility, there are further constraints that affect the shaft-power requirements of the generator. The minimum feasible generator shaft-power is the ability of the aircraft to maintain level flight. The developed model was used to obtain a minimum of 346 kW of installed SLS shaft power for the generator. Additionally, the time to charge the battery may be considered as a constraint, if a specified SOC needs to be reached before the end of the mission. For example, in order to be able to immediately continue flight operations with the aircraft after landing.

The minimum power-requirement for the generator to allow a sustained cruise at 160 KCAS (i.e. 175 KTAS at 6000 ft) is 804 kW. This cruise velocity is selected as a compromise between maximum allowable airspeed (structural limit) and specific range using the employed generator modelling.

Since charging time is not only depending on available generator power, but also on the size of the battery, an additional parameter study was performed with the developed model in cruise flight. The results are depicted in Figure 11 and show the charging time of a 500 kg battery (150 Wh/kg) from 10% to 100% SOC with varying cruise speed and generator power.
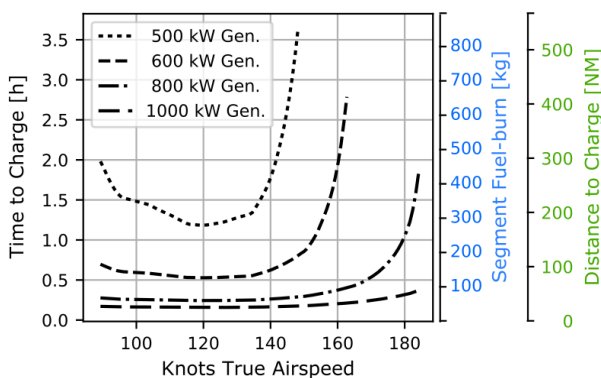

FIGURE 11. Time, fuel and distance to charge from 10% to 90% SOC for a retrofit with 500 kg battery and 804 kW of generator power, cruising at 160 KCAS (175 KTAS) and 6kft altitude.

The results show that, depending on the cruise speed, the charging time of the battery will be higher than 1 hour if a generator with less than 500 kW power is used. The result becomes less sensitive to this parameter for power-levels above 600 kW, where a minimum time to charge of about 30 minutes is possible for speeds around 120 KTAS. Depending on the available mission-fuel load, the fuel-burn during the charging cruise may also lead to further operational or sizing constraints. The same goes for the cruise distance that is required to recharge the batteries.

Assessing the results more generally leads to the conclusion that there is an important interaction regarding the size of the generator and that of the battery. This relationship should to be carefully studied at a later design stage.

There are many more constraints that could be investigated at this stage. Among these are minimum excess power at various points of the mission, battery reserves for electric go-around or maximum power requirements for climb segments. Investigating these, however, is out of the scope of this work but could definitely provide valuable insight.

4.5. Example Mission Results

In the following examples, the previously obtained results were used to define a design point for battery size and generator power. The mission profiles c) - e), as depicted in Figure 5, were then calculated with the selected hybrid-electric propulsion system sizing.

The generator shaft power was selected so that a cruise speed of 175 KTAS can be sustained at 6'000 ft altitude. This means, the battery state of charge may be kept constant while cruising at this speed and altitude (Figure 3b). Calculating required thrust with the developed performance mode at this point results in 804 kW of installed generator shaft-power at sea-level.

Using a vertical line through this point in Figure 10 and choosing a generator activation altitude of 4'000 ft results, with some margin for the altitude, in a battery mass of about 500 kg.

The aforementioned design point (804 kW, 500 kg) for the sizing of the propulsion system was used to calculate mission performance by using the methodology outlined in Section 2.

The profiles c) and d), as shown in Figure 5, are almost identical. Details have been explained in Section 3. The range results are shown in Figure 12. The calculation with 10% battery SOC after landing yields a range of 356 NM while the calculation with 90% SOC on landing yields 335 NM of range.
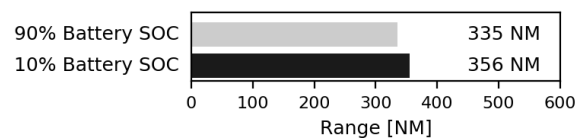

FIGURE 12. Calculated range of cruise missions with pure-electric propulsion used at altitudes below 4'000 ft. Results differ in charging-time during cruise to obtain a desired state-of-charge (SOC) at the end of the mission.

Figure 13 shows the simulated altitude, battery SOC, generator power and Knots TAS plotted over time. The altitude vs. time and speed vs. time plots are almost identical for both simulations. The only difference is the length of the cruise segment at about 110-120 minutes. In contrast, the profile plots of SOC vs time clearly show the origin of the difference in maximum range. The charging of the battery after the climb is finished takes about 30

min., that is one third of overall cruise time in the "90%"-mission (solid line). The charging segment of the "10%"-mission (dashed line) only takes about 5 minutes. The higher generator fuel flow during charge in the "90%"-mission is therefore the main cause for less maximum range. Note that the last 30 minutes of the simulation account for loiter reserves.

Although the presented range-results are highly dependent on chosen conditions, such as battery energy density, generator power, cruise speed and reserves, it is possible to say that the difference between the results are comparably small, only about 6%. This is operationally interesting as it could be possible to perform a silent take-off and climb up to 4'000 ft just after turning the aircraft around if the battery state-of-charge is 90% after landing.

The calculation of the profile depicted in Figure 5e yields an electric loiter time of about 12.5 minutes with a radius of action of 163 NM. Compared to the loiter endurance of the baseline aircraft, this performance is far inferior. The result can be explained by the low specific energy density of the battery (150 Wh/kg) in comparison to the properties of common aviation fuels (about 12'000 Wh/kg) [2].
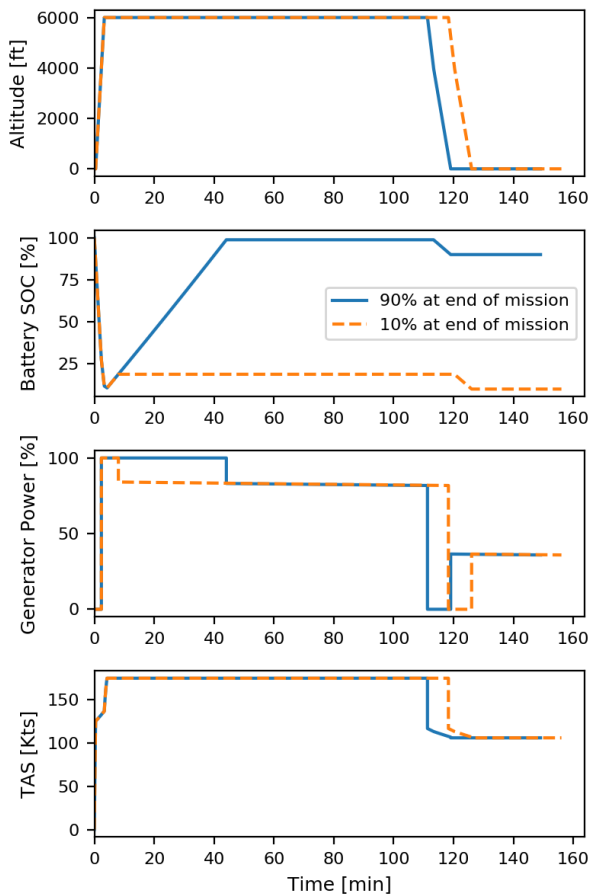

FIGURE 13. Calculation results of the cruise profiles from Figure 5c and d for altitude, battery SOC, generator power and speed plotted vs. time.

4.6. Performance Comparison of Retrofit and Baseline Aircraft

The mission performance of the retrofitted aircraft for the flight profile depicted in Figure 5d (90% SOC) together with the payload-range data of the Do-228NG is shown in Figure 14.
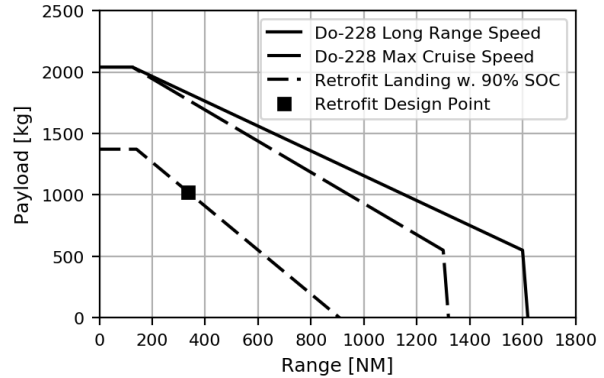

FIGURE 14. Payload-Range comparison of the Do-228NG [8] and the retrofitted model with 500 kg battery mass and 804 kW generator power cruising at 160 KCAS.

Comparing the obtained result to the performance of the Do-228NG reveals that the modeling of the current design point yields only about 30% (a minus of 70%) of the Do-228NG range at an identical payload of 50% (1020 kg). The retrofit is only capable of carrying about 56% of the payload that the Do-228NG is able to carry over the same distance.

Possible measures to improve the performance that was obtained here by assuming current technology levels could be enhancing the MTOW of the aircraft or using a battery system that provides a higher installed energy density, if available. Furthermore, the reduction of cruise speeds to reduce power requirements may be a viable option.

Besides the potential noise reduction of the presented, new propulsion concept, it has to be acknowledged that there are significant drawbacks in payload and range, mainly driven by the battery energy density.

5. CONCLUSION

This work describes a methodology based on a point-mass, segment-based mission performance simulation that allows for the analysis of hybrid-electric propulsion systems. The methodology was implemented in the Aircraft Performance Program APP. APP was coupled with the Python module pyAPP, to perform a sizing study and resulting mission performance analysis of a hybrid-electric retrofit of the RUAG Do-228NG, a 20 passenger-class aircraft. The results are then discussed and compared with the reference aircraft.

The retrofit study shows that the simulation of parts of flight profiles as well as full mission profiles does not only reveal relationships that are non-trivial but also essential to enable a sound system design. The low execution time

of the calculations allows for fast evaluation of changed design variables and their influence on the resulting performance. The flexibility provided by the scripting module allows comparably easy set-up of studies. These studies support the identification of constraints, for example fuel or time to charge, that are operationally relevant but not immediately visible or easy to estimate.

Finally, the successful application of the methodology to the sizing study of a hybrid-electric propulsion system renders it a valuable tool, not only during mission performance analysis and optimization, as was shown in [3], but also for aircraft or system-level design. Hence, the presented methodology and tool-chain is usable in multiple areas of aircraft component or system level design.

6. REFERENCES

[1] Langelaan, J. W., Green Flight Challenge: Aircraft Design and Flight Planning for Extreme Fuel Efficiency, Journal of Aircraft, Vol. 50, No. 3, 2013, DOI: 10.2514/1.C032022

[2] Hepperle, M., Electric Flight – Potential and Limitations, AVT-209 Workshop on Energy Efficient Technologies and Concepts of Operation, Lisbon, October 2012

[3] Immer, M., Juretzko, P., Advanced Aircraft Performance Analysis, accepted on 13-Mar-2017 in Journal of Aircraft Engineering and Aerospace Technology, DOI: 10.1108/AEAT-11-2016-0205.R2

[4] Darecki, M. et al., Flightpath 2050 Europe's Vision for Aviation, Report of the High Level Group on Aviation Research, Publications Office of the European Union, 2011, DOI: 10.2777/50266

[5] Airbus E-Fan Product Website, http://company.airbus.com/responsibility/airbus-e-fan-the-future-of-electric-aircraft.html, accessed 31.08.2017

[6] Pipistrel d.o.o., Taurus Electro Product Website, http://www.pipistrel.ca/Taurus_Electro/, accessed on 31.08.2017

[7] Siemens AG, Aerobatic Airplane "Extra 330LE", https://www.siemens.com/press/pool/de/events/2016/corporate/2016-12-innovation/inno2016-aerobatic-airplane-e.pdf, Press Release, 2016, accessed 31.08.2017

[8] RUAG Aerospace Services GmbH, Dornier 228 Advanced Commuter (AC) Facts & Figures, accessed 02.08.2017 via dornier228.ruag.com

[9] APP 6.0 User Manual, ALR Aerospace, Zurich, 2016

[10] APP 6.0 Technical Reference Manual, ALR Aerospace, Zurich, 2016

[11] Equations for calculation of International Standard Atmosphere and associated off-standard atmospheres, ESDU 77022, 1977

[12] Python 2.7, Python Software Foundation, Retrieved from https://www.python.org/

[13] Pipistrel d.o.o., Pipistrel Alpha Electro Technical Data, http://www.pipistrel.si/plane/alpha-electro/overview, accessed 31.08.2017

[14] Air Energy GmbH, Reference Projects, http://www.airenergy.de/en/referenzprojekte/solar-impulse-i/, accessed 31.08.217

[15] Petermaier, K., Electric propulsion components with high power densities for aviation, Transformative Vertical Flight Workshop, 08.03.2015

[16] Raymer, D., Aircraft Design: A Conceptual Approach, 5th edition, AIAA Educational Series, AIAA, Virginia, USA, 2012

7. ACKNOWLEDGEMENTS